

How robust the global measurements of London penetration depth are: the case of $\text{Fe}(\text{Te}_{1-x}\text{Se}_x)$

K. Cho,¹ H. Kim,^{1,2} M. A. Tanatar,¹ J. Hu,³ B. Qian,³ Z. Q. Mao,³ and R. Prozorov^{1,2,*}

¹*The Ames Laboratory, Ames, IA 50011, USA*

²*Department of Physics & Astronomy, Iowa State University, Ames, IA 50011, USA*

³*Department of Physics and Engineering Physics, Tulane University, New Orleans, LA 70118*

(Dated: 4 July 2011)

We report tunnel diode resonator measurements of in-plane London penetration depth, $\lambda(T)$, in optimally-doped single crystals of $\text{Fe}(\text{Te}_{0.58}\text{Se}_{0.42})$ with $T_c \sim 14.8$ K. Systematic measurements were carried out for six samples with different size and surface roughness. The power-law behavior, $\Delta\lambda(T) = AT^n$ was found for all samples with the average exponent $n_{avg} = 2.3 \pm 0.1$ and the pre-factor $A_{avg} = 1.0 \pm 0.2 \text{ nm/K}^{2.3}$. The average superfluid density is well described by the self-consistent two-gap γ model resulting in $\Delta_I(0)/k_B T_c = 1.93$ and $\Delta_{II}(0)/k_B T_c = 0.9$. By analyzing the data obtained on samples of different size and deliberately introduced surface roughness, it is concluded that the calibration procedure used to obtain $\lambda(T)$ from the measured TDR frequency shift is quite robust and the uncertainty in sample dimensions and the nature of surface roughness play only minor role. The exponent n , directly related to the superconducting gap structure, remains virtually unchanged. The calibration - dependent pre-factor A shows some variation, but stays within reasonable margin ruling out some recent suggestions that surface conditions can significantly affect the results. Our results confirm that precision global measurements provide the most objective information regarding temperature - dependent London penetration depth.

The crystals of iron-based superconductors are micaceous and soft, which prompts questions related to sample structure and homogeneity. Many measurements assume perfect uniformity of the bulk properties and perfectly flat surface. This is especially important for the measurements of London penetration depth, $\lambda(T)$, which is one of the key quantities that can be measured with great precision providing valuable information on the quasiparticle excitations, thus the superconducting gap structure. When the entire sample is measured, several factors may affect the outcome. Size and shape enter the calibration factors that is used to convert raw data into the actual length. Chemical inhomogeneity may affect the measurements as an intrinsic source. One recent example of the experimental controversy is the comparison of $\lambda(T)$ estimated from the tunnel-diode resonator (TDR) and first critical field measurements in single crystals of $\text{Fe}(\text{Se},\text{Te})$ [1]. In order to reconcile two data sets the authors had to assume that the effective sample dimension, R , in the TDR calibration should be five times larger than the calculated from the sample dimensions, presumably due to surface roughness.

In order to test the effects of sample size, shape and surface roughness we measured London penetration depth in optimally doped $\text{Fe}(\text{Te}_{0.58}\text{Se}_{0.42})$ with $T_c \sim 14.8$ K using a TDR technique. A series of measurements were carried out on parts of the same sample with different sizes and surface roughness. We find a robust power-law variation, $\lambda(T) \sim AT^n$ with $n = 2.3 \pm 0.1$ among all measurements indicating intrinsic behavior. For the purpose of investigating how surface roughness affects $\Delta\lambda(T)$, the edges of one of the samples were deliberately damaged by a blade, see Fig. 1. Measurements of this sample before

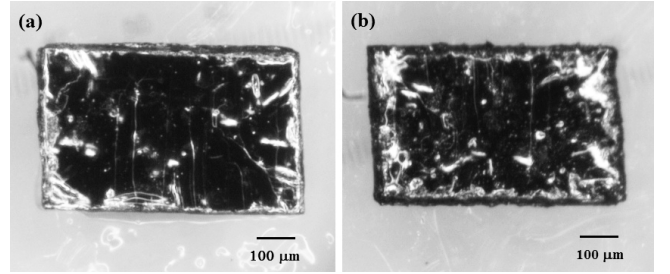


FIG. 1. (Color online) (a) Sample 2 - before and after (b) (Sample 2-R) deliberate roughening, see Table I

and after damaging the edges show no significant change of the pre-factor A or the exponent n . These results suggest that London penetration depth measured by a TDR technique represents an intrinsic quantity provided that the samples exhibit homogeneous superconductivity. We emphasize that it is the exponent n that is most important quantity to characterize the gap structure and possible pair-breaking effects.

The iron chalcogenide family of superconductors FeCh ($\text{Ch} = \text{Se/Te/S}$) was discovered in 2008 [2] shortly after the discovery of the first iron based superconductor $\text{La}(\text{O}_{1-x}\text{F}_x)\text{FeAs}$ [3]. The structure of this family is simpler than those of other Fe-based superconductors (FeSC) [4–7]. The square planar sheets of Fe ions are alternated by the distorted tetrahedra of Chalcogen ions. Even with simpler structure, the electronic structure of FeCh is similar to other FeSCs. Superconductivity in FeCh appears upon substitution of Te with Se or S [8, 9], or control of the amount of excess Fe [2, 11]. The superconducting transition temperature T_c is lower than those in most

TABLE I. List of samples and their physical constraints. R is the effective dimension calculated from the dimensions of a sample [10].

Sample	Dimensions (μm^3)	R (μm)	Edge condition
1	$712 \times 488 \times 40$	33.5	clean cut
1-A	$491 \times 270 \times 40$	22.6	clean cut
1-B	$489 \times 443 \times 40$	28.4	clean cut
2	$702 \times 455 \times 40$	32.8	clean cut
2-R	$680 \times 430 \times 40$	31.5	rough edge
2-R-C	$527 \times 421 \times 40$	28.6	clean cut

other FeSCs. In $\text{Fe}_y(\text{Te}_{1-x}\text{Se}_x)$ at optimal doping, T_c reaches a value of ~ 14 K and ~ 36 K under high pressure [2, 12–16]. A series of theoretical and experimental studies suggest that superconductivity in FeCh could be magnetically mediated following the spin-fluctuation picture [17–20].

The pairing mechanism of FeCh has been explored from various measurements [21, 22]. In nuclear magnetic resonance (NMR) study of polycrystalline FeSe ($T_c = 8$ K), the unconventional pairing was suggested from the absence of the NMR coherence peak in conjunction with the power-law temperature dependence of the spin-relaxation rate, $1/T_1 \sim T^3$ [21]. This can be explained with the unconventional order parameter such as a fully gapped s_{\pm} or a nodal gap pairing. In thermal conductivity measurements on FeSe_x single crystals, the multi-gap nodeless superconductivity was suggested [22].

The London penetration depth in FeCh has been measured by using different methods [1, 23–25]. The result from muon spin rotation (μSR) in FeSe_x is consistent with either anisotropic s -wave or a two-gap extended s -wave pairing [23]. Radio-frequency TDR measurements of $\lambda_{ab}(T)$ in $\text{Fe}_y(\text{Te}_{1-x}\text{Se}_x)$ ($x = 0.37$ [24], $x = 0.44$ [25], and $x = 0.45$ [1]) by three different groups found similar power-law exponent n and some variation in the pre-factor A : $n \sim 2.0$, $A \sim 3.7$ nm/K n [24], $n \sim 2.2$, $A \sim 0.9$ nm/K n [25] and $n \sim 2.0$, $A \sim 4$ nm/K n [1]. The full-range temperature behavior was also very similar. However, as mentioned above, an attempt to compare the TDR results with $\lambda(T)$ estimated from the measured first critical field, H_{c1} using Ginzburg-Landau formula (valid only at T_c) resulted in a large discrepancy forcing the Authors to suggest a very different effective dimension of $R = 70$ μm as compared to the one calculated from the sample dimensions, $R = 14$ μm [1].

Single crystals of $\text{Fe}(\text{Te}_{1-x}\text{Se}_x)$ were synthesized using a flux method as reported before [13]. The samples studied in this work had composition of Fe : Te : Se = 1.00 ± 0.01 : 0.58 ± 0.01 : 0.42 ± 0.01 determined from the energy dispersive x-ray spectroscopy (EDXS). Initially two samples 1 and 2 were prepared by careful

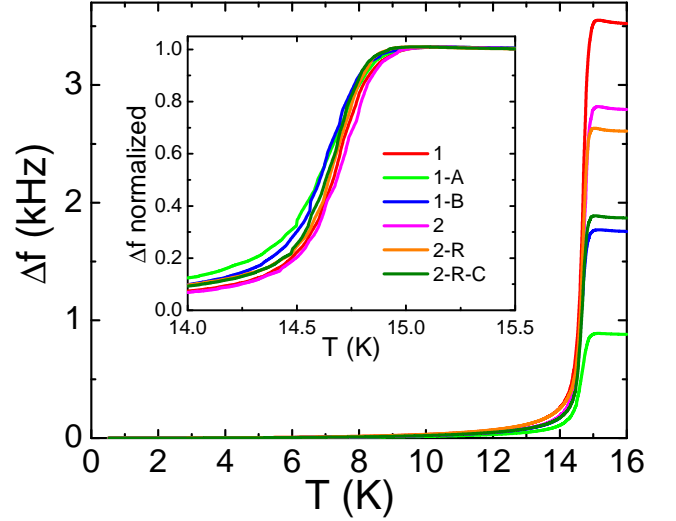


FIG. 2. (Color online) Temperature dependent frequency shift, $\Delta f(T)$ for each sample listed in Table I. T_c is consistently determined to be 14.8 K by using onset curves at the phase transition. Inset : $\Delta f(T)$ normalized based on the value at 16 K. The high temperature region is zoomed in showing the phase transition.

cleaving and cutting processes. Then Sample 1 was split into Samples 1-A and 1-B. To investigate the influence of the edge roughness, deliberate damage was done to Sample 2 by a razor blade. The original (Sample 2) and roughened ones (Sample 2-R) are shown in Fig. 1. To produce heaviest roughness possible, the damaging process was repeated multiple times resulting in a loss of about 10 % of volume. After the measurements, the rough surface of Sample 2-R was cut again as clean as possible to remove the roughness and the cleaned one was labeled as 2-R-C. The penetration depths was measured at each stage of the described procedures. The dimensions and edge condition of samples are summarized in Table I.

The in-plane London penetration depth, $\lambda(T)$, was measured using a self-oscillating tunnel-diode resonator (TDR) technique [10, 26, 27]. A sample under study is mounted on a sapphire rod and inserted into an inductor coil of a LC tank circuit. To measure the in-plane penetration depth, the sample is placed with its c -axis along the direction of ac-field (H_{ac}) induced by the inductor coil. Since $H_{ac} \sim 20$ mOe is weak enough ($\ll H_{c1}$), the sample is in the Meissner state, so its magnetic response is determined by the London penetration depth. The frequency shift in TDR, $\Delta f \equiv f(T) - f_0$, is used to obtain the magnetic susceptibility $\chi(T)$ from $\Delta f = -G4\pi\chi(T)$. Here $f_0 = 1/2\pi\sqrt{LC} \sim 14$ MHz is the resonant frequency of an empty resonator, $G = f_0 V_s / 2V_c(1 - N)$ is a geometric factor defined by the coil and sample volumes, V_c and V_s , and N is the demagnetization factor. Calibration constant G is directly measured by pulling the sample out of the coil at the lowest temperature. In the Meissner

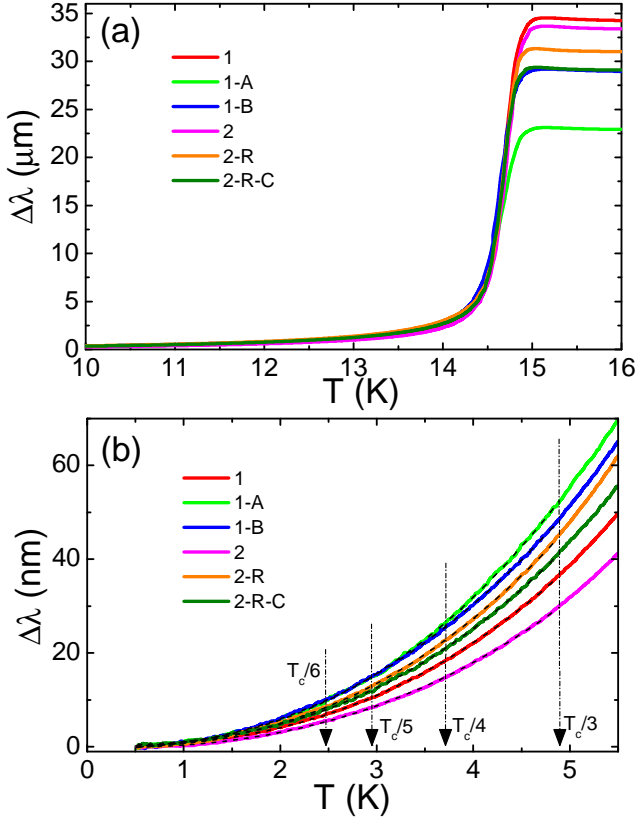


FIG. 3. (Color online) Temperature dependent penetration depth, $\Delta\lambda(T)$ for each sample. (a) High temperature region and (b) Low temperature region of $\Delta\lambda(T)$. The arrows indicate the upper-limits of fitting. The dashed lines are representative fits for each sample conducted up to $T_c/3$. All the fitting results are summarized in Fig. 4

state, λ can be obtained from the magnetic susceptibility, χ , following the relation $4\pi\chi = (\lambda/R)\tanh(R/\lambda) - 1$ where R is the effective dimension of the sample [10].

Figure 2 shows the raw data, temperature dependent frequency shift, $\Delta f(T)$, for samples listed in Table I. It is obvious that all the samples have quite sharp and well overlapping transition curves with the width of the superconducting transition of about ~ 0.3 K, so it seems that intrinsic superconducting properties were consistently reproducible between the samples (all samples come from the same large piece).

Above T_c the signal, $\Delta f(T)$, saturates due to two possible reasons. One, so-called sample-size-limited regime, is due to the size of a sample, which affects the $\tanh R/\lambda$ factor in the expression for the differential susceptibility. Another reason for the saturation, so-called skin-depth limited, occurs if the penetration depth becomes limited by the normal state skin depth. At T_c , the estimate value of the skin depth is about twice of that estimated from our calibration for $\lambda(T)$ [28]. Thus, the samples under current study is in sample-size-limited regime, so their penetration depth shifts, $\Delta\lambda(T)$, are cal-

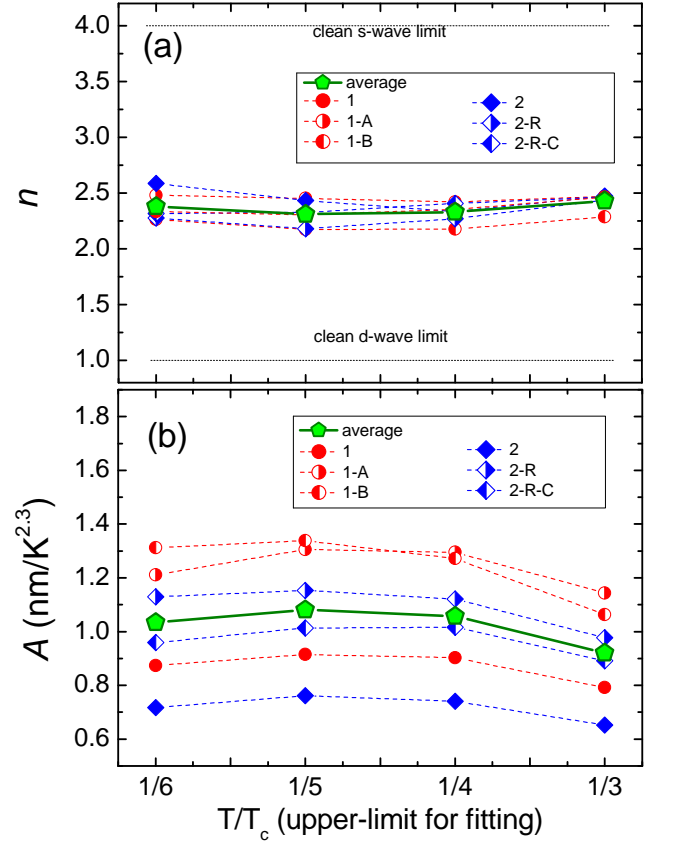


FIG. 4. (Color online) Results of the power-law fits to $\Delta\lambda(T) = AT^n$. Four different upper-limits, indicated by arrows in Fig. 3(b), were used. Panel (a): the exponent n , obtained by keeping A and n as free parameters. Panel (b): the pre-factor A , obtained at a fixed $n_{avg} = 2.3$, which is the average among all seven samples shown in Panel (a).

culated from $\Delta f(T)$ in Fig. 3 following the calibration procedure explained above. Figure 3(a) shows full temperature range which reveals sharp phase transitions at 14.8 K. The low temperature behavior of $\Delta\lambda$ is shown in Fig. 3(b). From these calibrated values we see that the penetration length in the normal state is comparable to the values of R , so we are in a sample-size limited regime. Therefore, the total frequency shift between the lowest temperature (~ 500 mK) and the normal state temperature ($T > T_c$), Δf_{total} , is related to the sample dimension. For instance, the largest Sample 1 has the biggest Δf_{total} and the smallest Sample 1-A the smallest Δf_{total} . The inset shows $\Delta f(T)$ normalized by the value at 16 K.

For quantitative analysis of the low temperature behavior, a power-law fit, $\Delta\lambda(T) = AT^n$ was performed for all six samples. To check how robust is the power law, in each case, four different upper temperature limits for the fit were used $T_c/3$, $T_c/4$, $T_c/5$ and $T_c/6$, shown schematically by arrows in Fig. 3(b). The results of the fitting are summarized in Fig. 4. Clearly, the fit coefficients remain

fairly constant with small (and expected) deviations at the lowest and the highest limits. Below we discuss the results for $T_c/4$ chosen as the upper limit for the fit.

As shown in Fig. 4 (a), in general, the exponent n is rather steady among all cases even though there are small variations. From the best fits with T/T_c upper limit, the average exponent $n_{avg} = 2.3 \pm 0.1$ is quite comparable to the previous reports of $n = 2.1$ [24], 2.2 [25] and 2.0 [1]. In conjunction with the superfluid density analysis discussed later, the exponent $n = 2.3$ can be explained by the nodeless two-gap pairing symmetry with strong pair breaking effect. The behavior of the pre-factor A is summarized in Fig. 4(b). Clearly, there is a very weak dependence on the fitting range, but there is a more substantial change between the samples. The average over all samples pre-factor $A_{avg} = 1.0 \pm 0.2 \text{ nm/K}^{2.3}$ is similar to other reports [24, 25].

Let us now try to understand the observed variation of A for different samples. We choose the values obtained from the fitting range up to $T_c/4$ where the fit quality was the best for all samples. We started by measuring Sample 1 that showed $A = 0.9 \text{ nm/K}^{2.3}$. After then Sample 1 was cut into Samples 1-A and 1-B. Every attempt was made to cut as clean as possible, but the pre-factor A has increased for both samples 1-A and 1-B to $1.3 \text{ nm/K}^{2.3}$. Although this change is not too significant, this result suggests that the effect of the rough edges becomes more pronounced as the sample size decreases. To estimate the effect of roughness itself when the size of a sample remains the same, Sample 2-R was made out of Sample 2 by deliberately damaging the edge with a razor blade. However, it turns out that the increment of A was only by $0.4 \text{ nm/K}^{2.3}$ from $0.7 \text{ nm/K}^{2.3}$ for Sample 2 to $1.1 \text{ nm/K}^{2.3}$ for Sample 2-R. This increment is similar to that between Sample 1 and two Samples 1-A and 1-B. This means that the intentional roughness created by coarse roughening a sample doesn't significantly affect the result and it also means that the effective sample dimension R used to calibrate the TDR data (so that it directly affects the pre-factor A) is very close to the calculated value. Otherwise, coarse roughening would make it many times larger due to the increased surface area exposed to the field. Furthermore, we tried to remove the rough surface from Sample 2-R by cutting the edges as clean as possible. The cleaned Sample 2-R-C showed that A has decreased by $0.1 \text{ nm/K}^{2.3}$ from that of Sample 2-R. This re-enforces our conclusion that surface roughness is not a dominant source determining A and plays only minor role. We also conclude that the explanation proposed to reconcile TDR and H_{c1} measurements [1] does not hold the ground. Instead, we think that the field of first penetration measured by the Hall-probe was determined by the surface barrier rather than H_{c1} . Finally, we conclude that global measurements provide a reliable estimate of the overall behavior of the London penetration depth by sampling all sample surfaces in contrast to the

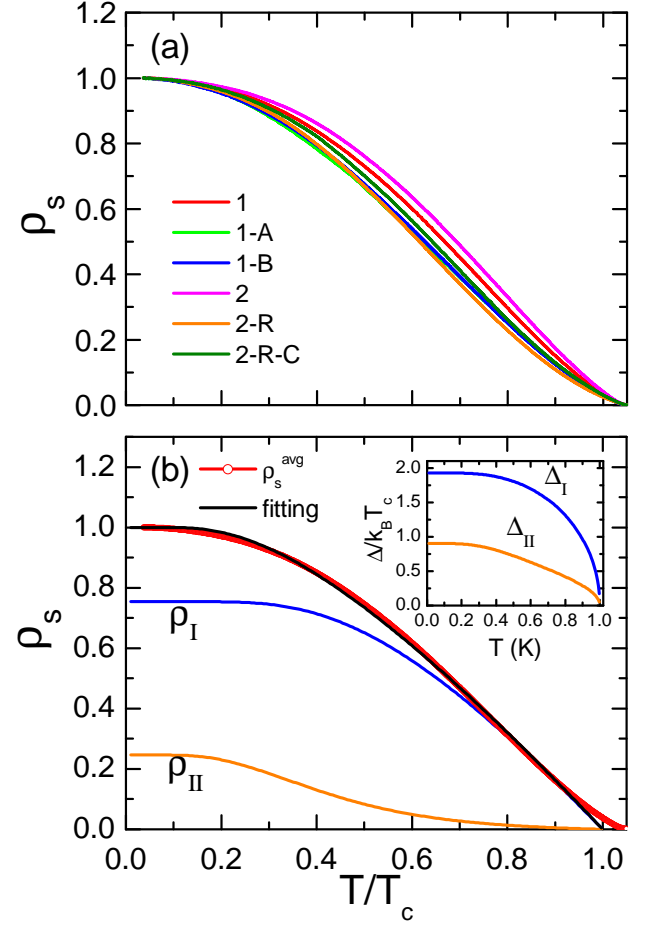


FIG. 5. (Color online) Superfluid density $\rho_s(T) = (\lambda(0)/\lambda(T))^2$ versus T/T_c . $\lambda(0) = 560 \text{ nm}$ obtained from the previous report [24]. (a) $\rho_s(T)$ for all six samples. (b) The average superfluid density for all six samples, ρ_s^{avg} (Red circle), is fitted to the two-gap γ model [29]. Black solid line is the fitting result with $\rho = \gamma\rho_I + (1 - \gamma)\rho_{II}$. The inset shows two gaps acquired from the fit, Δ_I and Δ_{II} .

local probes that are affected by the surface topography on the mesoscopic scale.

The superfluid densities $\rho_s = (\lambda(0)/\lambda(T))^2$ for all samples are shown in Fig. 5. The absolute penetration depth, $\lambda(0) = 560 \text{ nm}$ was determined by TDR measurements of Al-coated sample [24]. The variation of ρ_s among different samples is shown in Fig. 5 (a). For the purpose of fitting, the average ρ_s^{avg} is calculated from ρ_s of samples 1 and 2 which have lowest A values. The fitting was done with a self-consistent two-gap γ -model, where two gaps are calculated self-consistently at each temperature and at each iteration. The total superfluid density is given by $\rho = \gamma\rho_I + (1 - \gamma)\rho_{II}$ [29]. The partial densities of states are chosen to be equal on the two bands, $n_1 = n_2 = 0.5$ and Debye temperature of 230 K was used to calculate the experimentally observed $T_c = 14.8 \text{ K}$, which fixes the coupling constants (we used λ_{11}). Fig-

ure 5(b) demonstrates a good agreement between experimental ρ_s^{avg} (symbols) and fitting (black solid line). The parameters acquired from the fit are: $\lambda_{11} = 0.66$, $\lambda_{22} = 0.44$, $\lambda_{12} = 0.07$, $\lambda_{eff} = 0.34$, $\gamma = 0.75$ and $T_c = 14.95$ K. This result indicates that 75 % contribution of superfluid density comes from the band with ρ_I which has the larger gap Δ_I . The inset in Fig. 5 (b) shows the behaviors of two energy gaps Δ_I and Δ_{II} versus temperature. Clearly, the smaller gap has significantly non-BCS temperature dependence. The zero temperature energy gaps $\Delta_I(0)$ and $\Delta_{II}(0)$ are 2.5 meV ($\Delta_I(0)/k_B T_c = 1.93$) and 1.1 meV ($\Delta_{II}(0)/k_B T_c = 0.9$) respectively. The superconducting energy gaps has also been probed in different experiments. From μ SR [30, 31] and penetration depth [24] measurements, two s-wave energy gaps were reported with gap values similar to our results. μ SR studies in $\text{FeSe}_{0.5}\text{Te}_{0.5}$ [30, 31] revealed two gaps of $\Delta_{large} \sim 2.6$ meV and $\Delta_{small} \sim 0.5$ -0.87 meV, and the penetration depth study [24] also showed that $\Delta_{large} \sim 2.1$ meV and $\Delta_s \sim 1.2$ meV. According to scanning tunneling spectroscopy study, only one s-wave gap $\Delta \sim 2.3$ meV was observed in $\text{FeSe}_{0.4}\text{Te}_{0.6}$ [32], which is similar to the large gap $\Delta_I(0)$ of our result. However, rather large single or multi-gaps were reported from specific heat [33], optical conductivity [34], point-contact Andreev reflectivity [35], and angle-resolved photoemission spectroscopy [36] suggesting strong-coupling superconductivity. The electronic specific heat in $\text{Fe}(\text{Te}_{0.57}\text{Se}_{0.43})$ [33] revealed two energy gaps with $\Delta_{large} \sim 7.4$ meV and $\Delta_{small} \sim 5.0$ meV. From the optical conductivity in $\text{FeTe}_{0.55}\text{Se}_{0.45}$, two large energy gaps were also found with $\Delta_{large} \sim 5.1$ meV and $\Delta_{small} \sim 2.5$ meV. The point-contact Andreev reflectivity in $\text{FeTe}_{0.55}\text{Se}_{0.45}$ is consistent with single gap s-wave symmetry with Δ (at 1.70 K) ~ 3.8 meV. Angle-resolved photoemission spectroscopy in $\text{FeTe}_{0.7}\text{Se}_{0.3}$ [36], an s-wave single gap of $\Delta \sim 4$ meV was also observed. Overall, the pairing symmetry in $\text{FeTe}_{1-x}\text{Se}_x$ is still under debate.

To summarize, London penetration depth was measured in optimally-doped single-crystals of $\text{Fe}(\text{Te}_{0.58}\text{Se}_{0.42})$ of different size, shape and surface conditions to separate extrinsic and intrinsic effects determining the temperature variation of $\lambda(T)$. Even though there is a natural dispersion among six different samples, the average exponent n_{avg} and pre-factor A_{avg} are found to be 2.3 ± 0.1 and 1.0 ± 0.1 nm/K^{2.3}. The two-band γ model fits the superfluid density rather well resulting in $\Delta_I(0)/k_B T_c = 1.93$ and $\Delta_{II}(0)/k_B T_c = 0.9$. From comparison of six samples, it is found that there exists unavoidable micro(meso)-scopic surface roughness on the sample edges and the effect of the

roughness on pre-factor A becomes more important as the sample size decreases, whereas the exponent n remains practically unchanged. Overall, we conclude that global measurements provide an accurate and objective way to determine London penetration depth in pnictide superconductors.

The work at Ames was supported by the U.S. Department of Energy, Office of Basic Energy Sciences, Division of Materials Sciences and Engineering under contract No. DE-AC02-07CH11358. The work at Tulane was supported by the NSF under grants DMR-0645305 and EPS-1003897.

* Corresponding author: prozorov@ameslab.gov

- [1] T. Klein *et al.*, Phys. Rev. **B82**, 184506 (2010).
- [2] F. C. Hsu *et al.*, Proc. Natl. Acad. Sci. **105**, 14262 (2008).
- [3] Y. Kamihara *et al.*, J. Am. Chem. Soc. **128**, 10012 (2006).
- [4] M. Rotter *et al.*, Phys. Rev. Lett. **101**, 107006 (2008).
- [5] H. Ogino *et al.*, Supercond. Sci. Technol. **22**, 075008 (2009).
- [6] X. Zhu *et al.*, Phys. Rev. **B79**, 024516 (2009).
- [7] X. C. Wang *et al.*, Solid State Comm. **148**, 538 (2008).
- [8] K. W. Yeh *et al.*, Europhys. Letts. **84**, 37002 (2008).
- [9] Y. Mizuguchi *et al.*, J. Phys. Soc. Japan **78**, 074712 (2009).
- [10] R. Prozorov and R. W. Giannetta, Supercond. Sci. Technol. **19**, R41 (2006).
- [11] M. Bendele *et al.*, Phys. Rev. **B82**, 212504 (2010).
- [12] M. H. Fang *et al.*, Phys. Rev. **B78**, 224503 (2008).
- [13] T. J. Liu *et al.*, Phys. Rev. **B80**, 174509 (2009).
- [14] R. Khasanov *et al.*, Phys. Rev. **B80**, 140511(R) (2009).
- [15] S. Margadonna *et al.*, Phys. Rev. **B80**, 064506 (2009).
- [16] B. C. Sales *et al.*, Phys. Rev. **B79**, 094521 (2009).
- [17] A. Subedi *et al.*, Phys. Rev. **B78**, 134514 (2008).
- [18] T. L. Xia *et al.*, Phys. Rev. **B79**, 140510 (2009).
- [19] W. Bao *et al.*, Phys. Rev. Lett. **102**, 247001 (2009).
- [20] Y. Qiu *et al.*, Phys. Rev. Lett. **103**, 067008 (2009).
- [21] H. Kotegawa *et al.*, J. Phys. Soc. Jpn. **77**, 113703 (2008).
- [22] J. K. Dong *et al.*, Phys. Rev. **B80**, 024518 (2009).
- [23] R. Khasanov *et al.*, Phys. Rev. **B78**, 220510(R) (2008).
- [24] H. Kim *et al.*, Phys. Rev. **B81**, 180503(R) (2010).
- [25] A. Serafin *et al.*, Phys. Rev. **B82**, 104514 (2010).
- [26] T. Van Degrift *et al.*, Rev. Sci. Instrum. **46**, 599 (1975).
- [27] R. Prozorov *et al.*, Phys. Rev. **B62**, 115 (2000).
- [28] W. N. Hardy *et al.*, Phys. Rev. Lett. **70**, 3999 (1993).
- [29] V. G. Kogan *et al.*, Phys. Rev. **B80**, 014507 (2009).
- [30] P. K. Biswas *et al.*, Phys. Rev. **B81**, 092510 (2010).
- [31] M. Bendele *et al.*, Phys. Rev. **B81**, 224520 (2010).
- [32] T. Kato *et al.*, Phys. Rev. **B80**, 180507(R) (2009).
- [33] J. Hu *et al.*, Phys. Rev. **B83**, 134521 (2011).
- [34] C. C. Homes *et al.*, Phys. Rev. **B81**, 180508(R) (2010).
- [35] W. K. Park *et al.*, eprint arXiv:1005.0190.
- [36] K. Nakayama *et al.*, Phys. Rev. Lett. **105**, 197001 (2010).